Deflagrations and Detonations in Thermonuclear Supernovae

Vadim N. Gamezo,[1] Alexei M. Khokhlov,[2] and Elaine S. Oran[1]

[1]*Laboratory for Computational Physics and Fluid Dynamics, Naval Research Laboratory, Washington, D.C. 20375, USA*
[2]*Department of Astronomy and Astrophysics, University of Chicago, Chicago, Illinois 60637, USA*
(Received 16 January 2004; published 28 May 2004)

We study a type Ia supernova explosion using three-dimensional numerical simulations based on reactive fluid dynamics. We consider a delayed-detonation model that assumes a deflagration-to-detonation transition. In contrast with the pure deflagration model, the delayed-detonation model releases enough energy to account for a healthy explosion, and does *not* leave carbon, oxygen, and intermediate-mass elements in central parts of a white dwarf. This removes the key disagreement between simulations and observations, and makes a delayed detonation the mostly likely mechanism for type Ia supernovae.

Type Ia supernovae (SN Ia) are produced by thermonuclear explosions of white dwarf (WD) stars composed primarily of C and O nuclei and detached degenerate electrons. The most probable explosion scenario involves a binary star system, in which a WD can increase its own mass by accreting material from its companion until it approaches the Chandrasekhar limit, $1.4 M_\odot$. Near this limit, a small increase in mass results in substantial contraction and compression of the WD. The compression increases the temperature, accelerates nuclear fusion reactions, and triggers the thermonuclear runaway [1] that eventually ignites thermonuclear burning near the WD center. This starts a thermonuclear explosion that releases $\sim 10^{51}$ ergs during a few seconds. The energy is produced by a network of thermonuclear reactions that begins with the original ^{12}C and ^{16}O nuclei and ends in the formation of ^{56}Ni and other iron-group elements. Considerable amounts of intermediate-mass elements (IME), such as Ne, Mg, Si, S, and Ca, are created as well. Type Ia and other types of supernovae play an important role in stellar nucleosynthesis and in releasing the newly synthesized elements into interstellar medium, thus providing raw material for the next generations of stars and planets.

Because of their extreme and predictable luminosity, SN Ia are extensively used as standard candles to measure distances and estimate cosmological parameters critical for our understanding of the global evolution of the Universe. To improve these measurements, we need comprehensive theoretical and numerical models of SN Ia that describe details of the explosion and connect them to observed characteristics of SN Ia, such as spectra and light curves. One-dimensional (1D) numerical models have been extensively used to test general ideas about possible explosion mechanisms [2–7]. In particular, 1D models have ruled out the possibility of a thermonuclear detonation, a supersonic shock-induced combustion mode, as a sole mechanism for SN Ia explosions. A detonation propagating through a high-density WD produces mostly Ni and almost none of the IME observed in SN Ia spectra. One-dimensional models have also shown

that a detonation can produce IME if it propagates through a low-density WD preexpanded during the initial deflagration stage of the explosion. These delayed-detonation models [8–14], which have a deflagration-to-detonation transition (DDT) at some stage of the thermonuclear explosion, are the most successful in reproducing observed characteristics of SNe Ia. Many crucial physical details, however, including the mechanism of DDT and the turbulent flame structure, are missing by definition from 1D models because SN Ia explosions are intrinsically three-dimensional (3D) phenomena.

Full-scale 3D numerical simulations of thermonuclear supernova explosions have become a reality during the past few years [15–18]. They have shown, in particular, that the development of a turbulent thermonuclear flame in the gravitational field of a WD allows funnels of unburned and partially burned material to remain in the vicinity of the WD center until the end of the explosion. This would produce distinct signatures of low-velocity C, O, and IME in SN Ia spectra. As the observed spectra do not show these signatures, the deflagration model must be incomplete. Previously, we suggested [15,18] but did not prove that a detonation triggered by the turbulent flame could burn the remaining material near the WD center and make the model consistent with observations. Here, we test this hypothesis using a 3D numerical delayed-detonation model of SN Ia explosion in which a deflagration undergoes a transition to a detonation.

Input physics and numerical implementation.—The numerical model discussed in detail in [15,18] is based on reactive Euler equations that include gravity terms and are coupled with an equation of state for a degenerate matter and a simplified kinetics of energy release. The equations are integrated on a Cartesian adaptive mesh using an explicit, second-order, Godunov-type numerical scheme. The model describes compressible fluid dynamics on large scales in an exploding WD including the expansion of a star, Rayleigh-Taylor (RT) and Kelvin-Helmholtz instabilities, turbulence, pressure waves, shocks, and detonations. The nuclear kinetics is

approximated by a four-equation mechanism [8,15] that describes the energy release, consumption of C, nuclear statistical quasiequilibrium (NSQE or QSE) and nuclear statistical equilibrium (NSE) relaxations, and neutronization. The turbulent flame speed is provided by an additional subgrid model [15,18] that takes into account physical processes at scales smaller than the computational cell size. In particular, it assumes that turbulent burning on small unresolved scales is driven by the gravity-induced RT instability.

The model is able to reproduce the two different regimes of the thermonuclear burning in a WD, a subsonic deflagration and a supersonic detonation. These regimes differ by the mechanism of propagation of the reaction wave: A deflagration involves heat conduction or turbulent mixing, and a detonation involves shock compression. For both regimes, the energy is released by the same network of thermonuclear reactions, and the physical thickness of the reaction front strongly depends on density. It can be up to 12 orders of magnitude less than the WD radius R_{WD} for deflagrations [19,20] and up to 10 orders of magnitude less than R_{WD} for detonations [21,22]. Since the large-scale simulations described here do not resolve length scales smaller than $10^{-3}R_{WD}$, the reaction fronts at high densities are still unresolved. We explicitly resolve only parts of the reaction zone associated with NSE relaxation that become very large at low densities and cause an incomplete burning that produces Si and other IME. Resolution tests show that the minimum computational cell size $dx_{min} = 2.6 \times 10^5$ cm used here for the deflagration stage and $dx_{min} = 10.4 \times 10^5$ cm used for the detonation stage are adequate for this type of simulation.

Deflagration stage.—The initial conditions for the deflagration stage model a $1.4 M_\odot$ WD in hydrostatic equilibrium with initial radius $R_{WD} = 2 \times 10^8$ cm, initial central density $\rho_c = 2 \times 10^9$ g/cm^3, spatially uniform initial temperature $T = 10^5$ K, and uniform initial composition with equal mass fractions of ^{12}C and ^{16}O nuclei. The burning was initiated at the center of WD by filling a small spherical region at $r < 0.015 R_{WD}$ with hot reaction products without disturbing the hydrostatic equilibrium. We model one octant of the WD assuming mirror symmetry along the $x = 0$, $y = 0$, and $z = 0$ planes. The computational domain is a cube with a side of $x_{max} = 5.35 \times 10^8$ cm.

The development of the thermonuclear flame was described in detail earlier [18]. The initially spherical flame propagates outwards with a laminar velocity ~ 100 km/s, becomes distorted due to the RT instability, and forms multiple plumes at different scales. Buoyancy causes the hot, burned, low-density material inside the flame plumes to rise towards the WD surface. The same gravitational forces also pull the cold, unburned, high-density material between the plumes down towards the center. The flame becomes turbulent and forms a dynamic convoluted surface penetrated in all directions

by very irregular funnels of unburned and partially burned material.

The highly developed 3D flame surface increases the burning rate and improves the estimation of energy release compared to 1D and 2D deflagration models. The intense convection on large scales also causes the burned material to spend less time in high-density central parts of WD, thus reducing the neutronization [15]. The same convective flows, however, bring unburned material to the central parts of the exploding star. As a result, substantial amounts of C, O, and IME remain near the WD center by the end of the explosion. As we have shown [15,18], this makes predictions of the 3D deflagration model inconsistent with observed spectra of SN Ia.

Detonation stage.—The disagreement between predictions from the pure deflagration simulation and observations strongly suggests that the turbulent flame in SN Ia triggers a detonation. The process of DDT involves events occurring at small scales that are comparable to the detonation wave thickness, and, thus, cannot be directly modeled in large-scale simulations. To study the effects of a detonation, we therefore assume a time and a location for DDT. (A similar approach has been used previously in 1D [8–13] and 2D [23–25] delayed-detonation models.) Now the deflagration results are initial conditions, and we impose a hot spot to ignite the detonation. The time and location for the detonation initiation are parameters that can be varied and optimized. Here, we explore the three cases (a), (b), and (c) defined below.

Case (a) corresponds to central detonation initiation at 1.62 s after the beginning of the deflagration. By that time, 1/3 of WD mass has burned, the WD radius has increased by a factor of 1.55, and the density of unburnt material near the center has dropped to 2.5×10^8 g/cm^3. A detonation at this density produces mostly Ni and propagates outwards at $\sim 12\,000$ km/s, which is comparable to the expansion velocities induced by subsonic burning. When the detonation reaches unburned material with density below $(1–5) \times 10^7$ g/cm^3, it begins to produce IME. Different parts of the detonation front that exit different funnels collide with each other, coalesce, and eventually reach the surface of the star.

The detonation transforms all C and O in central parts of the WD into iron-group elements, and produces IME in outer layers. This drastically changes the distribution of nuclei compared to that produced by the pure deflagration. Funnels of unburned C and O disappear from central parts of the WD. Iron-group elements form a distinct core surrounded by a layer of IME. Angle-averaged mass fractions of the main elements calculated for the deflagration and the delayed-detonation models are compared in Fig. 1.

Similar results were obtained for the delayed-detonation case (b), for which the detonation was initiated at 1.62 s at 10^8 cm off center and produced a moderate asymmetry in composition. The results indicate that, during the period of detonation propagation, the
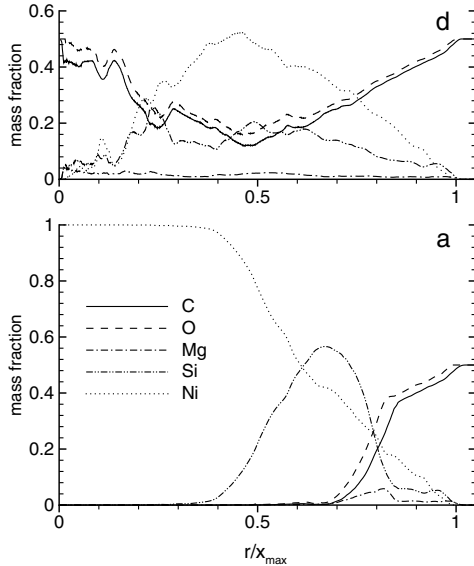
FIG. 1. Angle-averaged mass fractions of the main elements as functions of scaled distance from the WD center produced by the deflagration (d) and delayed-detonation (a) models at 1.94 s after the beginning of the explosion. The delayed-detonation model corresponds to case (a) described in the text. $x_{max} = 5.35 \times 10^8$ cm. Lines marked as Mg, Si, and Ni represent estimated cumulative mass fractions of elements from Ne to Mg, Si to Ca, and Ti to Ni, respectively. The estimations are based on a four-equation nuclear kinetic scheme [15,18] and the reaction zone structure of a 1D detonation wave calculated in [21] with a detailed nuclear kinetics.

density of the expanding unreacted material ahead of the shock can decrease by an order of magnitude compared to its value at the end of the deflagration stage. Because the detonation burns material to different products at different densities, it can create a large-scale asymmetry in composition if it starts far from the WD center. A similar conclusion based on 2D simulations was made in [25].

The asymmetry effect in our simulations is limited because we calculate only one octant of a WD and impose mirror boundary conditions. The degree of asymmetry would increase if the simulations were performed for a full star. Then the second mirror-reflected spot for detonation initiation would be eliminated. Three-dimensional simulations [15,26] also show that a developing flame, unrestricted by mirror boundaries, can move away from the WD center, thus creating a large-scale asymmetry at very early stages of the explosion.

For case (c), the detonation was initiated at the WD center at 1.51 s when 1/4 of WD mass has burned, the WD radius has increased by a factor of 1.30, and the density of unburnt material near the center has decreased to 4.4×10^8 g/cm^3. Case (c) produced more iron-group elements than cases (a) and (b) because the detonation propagated through higher-density material. The earlier detonation initiation also resulted in a faster explosion that released 15% more energy. Total energies for all three cases and the deflagration model are shown in Fig. 2 as functions of
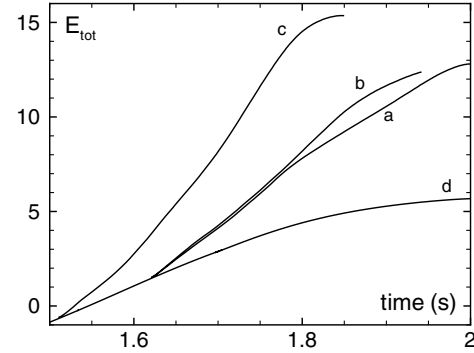
FIG. 2. Total energy as a function of time for deflagration (d) and delayed-detonation cases (a), (b), and (c) described in the text. Energy units are 10^{50} ergs.

time. The total energy E_{tot} here is the difference between the energy released by thermonuclear reactions and the binding energy of the star. Eventually E_{tot} will be transformed into kinetic energy of expanding material that can be measured in observations of SN Ia.

Figure 2 shows that the total energy released by delayed-detonation models, $(1.3–1.6) \times 10^{51}$ ergs, is much higher than the energy released by the deflagration model $\sim 0.6 \times 10^{51}$ ergs. The reason for this is that the deflagration is able to burn only about a half of the WD mass. The rest of the material expands to the densities below $\simeq 10^6$ g/cm^3 that do not support the thermonuclear burning. A detonation propagates faster and burns almost all of the WD mass before the material expands to low densities. The total energy released by the delayed-detonation models is in agreement with a typical range $(1–1.5) \times 10^{51}$ ergs obtained from SN Ia observations [7].

Discussion and conclusions.—Figure 1 shows the averaged distribution of elements at 1.94 s, the time when the WD surface reached the computational domain boundary, but the detonation did not yet reach the WD surface. At this time, the detonation front propagates through low-density outer layers of the star and produces mostly IME. All iron-group elements have already formed at higher densities. The total mass of iron-group elements created by the explosion is 0.78, 0.73, and 0.94 solar masses ($M_\odot$) for delayed-detonation cases (a), (b), and (c), respectively. Most of this mass is the radioactive ^{56}Ni that provides the energy source for the observed luminosity of SN Ia. The mass of ^{56}Ni estimated from observational data is about $0.6M_\odot$ for a typical SN Ia [27], and is in agreement with the total mass of iron-group elements produced by delayed-detonation models. For the deflagration model, the total mass of iron-group elements is only $0.47M_\odot$, which is insufficient to account for the luminosity of a typical SN Ia.

The carbon-oxygen layer that remains between the detonation front and the WD surface will continue to burn as the detonation advances. Oxygen in outer layers, which expand to densities below $\simeq 10^6$ g/cm^3 before the detonation reaches them, will remain unburned. Carbon

is likely to remain unburned for densities below $(1–3) \times 10^5$ g/cm^3. Unburned C and O in outer layers would produce spectral signatures only in the high-velocity range.

There are possibilities, however, for a delayed detonation to leave small amounts of C and O in inner parts of WD. For example, a detonation propagating through a thin, sinuous funnel of unburned material can fail if the funnel makes a sharp turn. A developing turbulent flame can also disconnect some funnels from the rest of the unburned material, thus creating unburned pockets that cannot be directly reached by a detonation wave. These pockets may or may not ignite when strong shocks generated by detonations reach them. The cellular structure of thermonuclear detonations in carbon-oxygen matter [22], and the ability of cellular detonations to form pockets of unburned material that extend far behind the 1D reaction zone, can also contribute into incomplete burning. All these phenomena occur at length scales comparable to the reaction zone thickness that are not resolved in large-scale simulations reported here, and require additional studies.

There have recently been efforts to detect low-velocity C in SN Ia spectra that could result from the funnels of unburned material near the WD center [28]. The results [28] indicate that C can be present at velocities 11 000 km/s. Even though this velocity is much lower than 20 000–30 000 km/s usually attributed to C in SN Ia spectra [29–31], it is still too high for the ejecta formed from central parts of a WD. For C and O, spectral signatures are difficult to observe, and estimated velocities of these elements are subject to large uncertainties. Intermediate-mass elements, however, produce distinct spectral lines and their velocities are well defined. The minimum observed velocities for IME [28,32] are large enough (∼10 000 km/s for Si) to rule out the presence of IME near the WD center, as is predicted by the deflagration model. A discussion on this subject can also be found in the recent article [33].

Figure 1 shows that, in contrast with the 3D deflagration model, the 3D delayed-detonation model of SN Ia explosion does *not* leave C, O, and IME in central parts of a WD. This removes the key disagreement between simulations and observations, and makes the 3D delayed detonation a promising mechanism for SN Ia explosion. Further analysis of 3D delayed detonations on a large scale requires 3D radiation transport simulations to produce spectra, and a detailed comparison between the calculated and observed spectra of SN Ia for different initiation times and locations. The uncertainty in detonation initiation can be eliminated only by solving the DDT problem that involves physical processes at small scales.

[1] F. Hoyle and W. A. Fowler, Astrophys. J. **132**, 565 (1960).
[2] W. D. Arnett, Astrophys. Space Sci. **5**, 180 (1969).
[3] C. J. Hansen and J. C. Wheeler, Astrophys. Space Sci. **3**, 464 (1969).
[4] K. Nomoto, D. Sugimoto, and S. Neo, Astrophys. Space Sci. **39**, L37 (1976).
[5] K. Nomoto, F.-K. Thielemann, and K. Yokoi, Astrophys. J. **286**, 644 (1984).
[6] S. E. Woosley and T. A. Weaver, Annu. Rev. Astron. Astrophys. **24**, 205 (1986).
[7] J. C. Wheeler, R. P. Harkness, A. M. Khokhlov, and P. A. Höflich, Phys. Rep. **256**, 211 (1995).
[8] A. M. Khokhlov, Astron. Astrophys. **245**, 114 (1991).
[9] H. Yamaoka, K. Nomoto, T. Shigeyama, and F.-K. Thielemann, Astrophys. J. **393**, L55 (1992).
[10] A. M. Khokhlov, E. Müller, and P. A. Höflich, Astron. Astrophys. **270**, 223 (1993).
[11] P. A. Höflich, Astrophys. J. **443**, 89 (1995).
[12] P. A. Höflich, A. M. Khokhlov, and J. C. Wheeler, Astrophys. J. **444**, 831 (1995).
[13] P. A. Höflich and A. M. Khokhlov, Astrophys. J. **457**, 500 (1996).
[14] J. C. Niemeyer and S. E. Woosley, Astrophys. J. **475**, 740 (1997).
[15] A. M. Khokhlov, astro-ph/0008463.
[16] M. Reinecke, W. Hillebrandt, and J. C. Niemeyer, Astron. Astrophys. **386**, 936 (2002).
[17] M. Reinecke, W. Hillebrandt, and J. C. Niemeyer, Astron. Astrophys. **391**, 1167 (2002).
[18] V. N. Gamezo, A. M. Khokhlov, E. S. Oran, A. Y. Chtchelkanova, and R. O. Rosenberg, Science **299**, 77 (2003).
[19] F. X. Timmes and S. E. Woosley, Astrophys. J. **396**, 649 (1992).
[20] A. M. Khokhlov, E. S. Oran, and J. C. Wheeler, Astrophys. J. **478**, 678 (1997).
[21] A. M. Khokhlov, Mon. Not. R. Astron. Soc. **239**, 785 (1989).
[22] V. N. Gamezo, J. C. Wheeler, A. M. Khokhlov, and E. S. Oran, Astrophys. J. **512**, 827 (1999).
[23] D. Arnett and E. Livne, Astrophys. J. **427**, 315 (1994).
[24] D. Arnett and E. Livne, Astrophys. J. **427**, 330 (1994).
[25] E. Livne, Astrophys. J. **527**, L97 (1999).
[26] A. C. Calder *et al.*, astro-ph/0405162.
[27] D. Branch and A. M. Khokhlov, Phys. Rep. **256**, 53 (1995).
[28] D. Branch *et al.*, Astron. J. **126**, 1489 (2003).
[29] R. P. Kirshner *et al.*, Astrophys. J. **415**, 589 (1993).
[30] A. Fisher, D. Branch, P. Nugent, and E. Baron, Astrophys. J. **481**, L89 (1997).
[31] P. A. Mazzali, Mon. Not. R. Astron. Soc. **321**, 341 (2001).
[32] A. V. Filippenko, Annu. Rev. Astron. Astrophys. **35**, 309 (1997).
[33] D. Branch, astro-ph/0310685.